Electronic Supplementary Information for publication: Metastability and polymorphism in dihydroxybenzenes – implications for thermal energy storage

Tomas S. Northam de la Fuente and Kalith M. Ismail
Materials Physics Center, CSIC-UPV/EHU, Paseo de Manuel Lardizabal 5, 20018 Donostia - San Sebastian, Spain

Mattia Gaboardi
Materials Physics Center, CSIC-UPV/EHU, Paseo de Manuel Lardizabal 5, 20018 Donostia - San Sebastian, Spain and Chemistry Department, University of Pavia & C.S.G.I., 27100 Pavia, Italy.

Valerio Di Lisio
Donostia International Physics Center (DIPC), Paseo de Manuel Lardizabal 4, 20018 Donostia - San Sebastian, Spain.

Daniele Cangialosi and Pedro B. Coto
Materials Physics Center, CSIC-UPV/EHU, Paseo de Manuel Lardizabal 5, 20018 Donostia - San Sebastian, Spain and Donostia International Physics Center (DIPC), Paseo de Manuel Lardizabal 4, 20018 Donostia - San Sebastian, Spain.

Alberto Otero-de-la-Roza
Departamento de Química Física y Analítica, Facultad de Química, Universidad de Oviedo, 33006 Oviedo, Spain.

Felix Fernandez-Alonso
*Materials Physics Center, CSIC-UPV/EHU, Paseo de Manuel Lardizabal 5, 20018 Donostia - San Sebastian, Spain; Donostia International Physics Center (DIPC), Paseo de Manuel Lardizabal 4, 20018 Donostia - San Sebastian, Spain; and IKERBASQUE, Basque Foundation for Science, Plaza Euskadi 5, 48009 Bilbao, Spain**

* Correspondence email address: pedro.brana@csic.es, felix.fernandez@ehu.eus

S1. EXPERIMENTAL DETAILS

o-dHBZ, *m*-dHBZ, and *p*-dHBZ were purchased from Sigma Aldrich and subsequently sublimated *in-vacuo*. Thermal Gravimetric Analysis (TGA) was performed using a Q500 system from TA Instruments. The *Hi-Res - Dynamic* protocol was used under dry-nitrogen atmosphere using a gas-flow rate of 40 mL min^{-1}. Measurements were performed with a starting mass of 14 mg for all three samples and heating from room temperature to 573 K – see Fig. S2 below. For *o*-dHBZ, a strong single peak in the weight-loss rate is observed at 375 K, in good agreement with a literature value of 377 K [1]. For *p*-dHBZ, a significant weight loss is observed at 420 K, starting 25 K below melting. *m*-dHBZ displays two main TGA peaks centered at 407 K and 418 K. As both lie above the melting point, this behaviour is suggestive of a stronger stability of the liquid compared to the other two isomers [1].

Temperature-modulated Differential Scanning Calorimetry (TM-DSC) measurements were performed using a Q2000 system from TA Instruments equipped with an intra-cooler to operate over the requisite temperature range under a dry-nitrogen atmosphere and using a gas-flow rate of 50 mL min^{-1}: 273–393 K for *o*-dHBZ; 273-423 K for *m*-dHBZ; and 353-473 K for *p*-dHBZ. All measurements were performed in "modulation mode" to obtain both reversing and non-reversing contributions to the heat flow and associated heat capacity. [2] Samples were prepared by hermetically sealing 6 to 10 mg of powder in Aluminium pans. Measurements were recorded at a constant heating rate of 2 K min^{-1} while changing the cooling rate between 1 K min^{-1} and 20 K min^{-1} (see Fig. S3 below and Fig. 2 in the main manuscript). All measurements were performed under temperature modulation to separate reversing and non-reversing contributions to the heat flow and heat capacity. The modulation frequency and amplitude were set to ensure heat-only conditions. Modulation amplitudes were sufficiently small to ensure measurements in heating-only mode. Instrumental uncertainties were found to be ± 10 μW, in line with the specifications provided by the manufacturer [3]. These values are well below measured signals and, therefore, no error bars have been included in the reported TM-DSC data. The standard deviations presented in Table II were obtained from three separate runs. As such, they provide a measure of potential systematic uncertainties associated with these measurements.

Fast Scanning Calorimetry (FSC) was performed with a Mettler–Toledo Flash DSC2+ unit equipped with a Huber intracooler and operated between 183 and 460 K. The FSC system comprises a Leica M60 optical microscope with 400X magnification. The sample chamber was purged with dry nitrogen at a flow rate of 20 mL min^{-1}. Initial measurements of dHBZs were performed by direct deposition of a sample mass of about 200-300 ng directly onto a Mettler–Toledo UFS1 chip (after preliminary conditioning of the chip and thermocouple correction). Temperature calibration was carried out using the melting point of an Indium standard (429.8 K) and the order-disorder transition of fullerene C_{60} ($\sim$260 K). For the measurement of *o*-dHBZ and *p*-dHBZ, samples were first melted at 1000 K s^{-1} and then covered by a thin layer of polydimethylsiloxane (PDMS supplied by Merck, viscosity of 10^5 cP) with the dual effect of improving heat transfer and reducing sample evaporation over cycling [4]. Since both *o*-dHBZ and *p*-dHBZ progressively evaporate upon cycling at high temperature, the FSC data were re-normalized at every cycle to the varying mass of the sample using the ratio between the area of the melting peak measured via FSC at every cycle and that measured by TM-DSC. For *m*-dHBZ, it was possible to sputter a thin layer of gold to seal the specimen and suppress evaporation [5]. The experiment displayed in Fig. S5 was obtained on a gold-sealed specimen by melting the sample well above T_m, followed by an isotherm and quenching of the liquid at various cooling rates (q_c=0.1-1000 K s^{-1}), followed by constant heating at 1000 K s^{-1}. The fictive temperature (T_f) was calculated using the Moynihan method, as described in Ref. [6], and fitted to the Vogel-Fulcher-Tammann (VFT) equation:

$$\tau^{-1} = \tau_0^{-1} \cdot \exp(-D \cdot T_0/(T_f - T_0)) \tag{1}$$

As shown in the inset of Fig. S5, this equation describes the data adequately, with a super-Arrhenius temperature dependence above the Vogel temperature T_0=215.6$\pm$0.2 K, a characteristic time of the process τ_0=2.6$\pm$3.0$\cdot 10^{-12}$ s, and a fragility index D=4.2$\pm$0.2. In particular, the latter index D indicates that *m*-dHBZ is a "fragile" glass former, according to the Angell classification (*i*.e., the supercooled liquid displays a strong temperature dependence of the relaxation timescale τ) [7]. The validity of the VFT equation to describe *m*-dHBZ tells us that the glass transition can be modeled as a single relaxation process.

S2. COMPUTATIONAL DETAILS

Density-functional-theory calculations [8] were carried out using the B86bPBE-XDM exchange-correlation functional,[9–

13] periodic boundary conditions, and the Projector Augmented Wave (PAW) method [14]. PAW datasets with 4 (C), 6 (O), and 1 (H) valence electrons were obtained from the pslibrary.[15] A plane-wave(density cutoff) of 80(800) Ry was used all throughout. Crystal-structure relaxation was carried out using the structures given in Table I as starting point. During structural optimization, both lattice parameters and atomic positions within the unit cell were relaxed. The structural relaxation was stopped when all the forces on the atomic coordinates and the lattice parameters were below 0.005 $^{eV}/_{\mathring{A}}$. For the monomers, we used periodic boundary conditions with a 20 Å cubic box and a single k-point at the origin in reciprocal space. Hydroxyl-group torsional energy profiles were calculated relaxing the structures for every value of the H-O-C-C dihedral angle in 10^{o} steps. The all-electron density was obtained using the PAW reconstruction. Non-covalent index (NCI) maps [16, 17] as well as the electron-density critical points were obtained using the critic2 program [18]. The latter used the recently developed "smoothrho" interpolation scheme.[19] Table III and Figs. S8-S13 below provide a comparison between experimental data and these calculations.

[1] W. Acree, Jr. and J. S. Chickos, J. Phys. Chem. Ref. Data **45**, 033101 (2016).
[2] B. Wunderlich, A. Boller, I. Okazaki, and K. Ishikiriyama, Thermochim. Acta **304-305**, 125 (1997), temperature Modulated Calorimetry.
[3] R. Marinescu and M. Mincu (Institute for Nuclear Research - Pitesti, Romania, 2015) mATERIALS SCIENCE.
[4] J. E. K. Schawe and S. Pogatscher, in *Fast Scanning Calorimetry* (Springer International Publishing, 2016) pp. 3–80.
[5] V. Di Lisio, B. Braunewell, C. Macia-Castello, M. Simoni, R. Senesi, F. Fernandez-Alonso, and D. Cangialosi, Thermochim. Acta **719**, 179414 (2023).
[6] C. T. Moynihan, P. B. Macedo, C. J. Montrose, C. J. Montrose, P. K. Gupta, M. A. DeBolt, J. F. Dill, B. E. Dom, P. W. Drake, A. J. Easteal, P. B. Elterman, R. P. Moeller, H. Sasabe, and J. A. Wilder, Ann. N. Y. Acad. Sci. **279**, 15 (1976).
[7] C. Angell, J. Non Cryst. Solids **131-133**, 13 (1991).
[8] E. Engel and R. M. Dreizler, *Density Functional Theory* (Springer Berlin Heidelberg, 2011).
[9] A. D. Becke, J. Chem. Phys. **85**, 7184 (1986).
[10] J. P. Perdew, K. Burke, and M. Ernzerhof, Phys. Rev. Lett. **77**, 3865 (1996).
[11] E. R. Johnson, in *Non-covalent Interactions in Quantum Chemistry and Physics*, edited by A. Otero-de-la Roza and G. A. DiLabio (Elsevier, 2017) Chap. 5, pp. 169–194.
[12] A. D. Becke and E. R. Johnson, J. Chem. Phys. **127**, 154108 (2007).
[13] A. Otero-de-la-Roza and E. R. Johnson, J. Chem. Phys. **136**, 174109 (2012).
[14] P. Blöchl, Phys. Rev. B **50**, 17953 (1994).
[15] A. Dal Corso, Comput. Mater. Sci. **95**, 337 (2014).
[16] E. R. Johnson, S. Keinan, P. Mori-Sánchez, J. Contreras-García, A. Cohen, and W. Yang, J. Am. Chem. Soc. **132**, 6498 (2010).
[17] A. Otero-de-la-Roza, E. R. Johnson, and J. Contreras-García, Phys. Chem. Chem. Phys. **14**, 12165 (2012).
[18] A. Otero-de-la-Roza, E. R. Johnson, and V. Luaña, Comput. Phys. Commun. **185**, 1007 (2014).
[19] A. Otero-de-la Roza, J. Chem. Phys. **156**, 224116 (2022).
[20] C. J. Brown, Acta Cryst. **21**, 170 (1966).
[21] S. P. Verevkin and S. A. Kozlova, Thermochim. Acta **471** (2008), 10.1016/j.tca.2008.02.016.
[22] Y. Ebisuzaki, L. H. Askari, A. M. Bryan, and M. F. Nicol, J. Chem. Phys. **87**, 6659 (1987).
[23] H. Wunderlich and D. Mootz, Acta Crystallogr. B. Struct. Sci. Cryst. Eng. Mater. **27**, 1684 (1971).
[24] M. D. Ossowska-Chruściel, E. Juszyńska-Gałązka, W. Zając, A. Rudzki, and J. Chruściel, J. Mol. Struct. **1082**, 103 (2015).
[25] S. C. Wallwork and H. M. Powell, J. Chem. Soc., Perkin Trans. 2 (1980), 10.1039/p29800000641.
[26] Y. Lee, J.-W. Lee, H.-H. Lee, D. R. Lee, C.-C. Kao, T. Kawamura, Y. Yamamoto, and J.-H. Yoon, J. Chem. Phys. **130**, 112031 (2009).

Table I: Summary of the known properties of the three dHBZ isomers in their condensed phases: melting point (T_m) and enthalpy (ΔH_m); crystallographic space group at room temperature; formula-unit volume (V_{fu}); and crystal density (ρ).

Isomer	T_m (K)	ΔH_m (kJ mol^{-1})	Space group	V_{fu} (Å^3)	ρ (g cm^{-3})	Refs.
ortho	377.7	22.0–22.9	$P2_1/c$	128.4	1.34	[1, 20, 21]
meta	383	20.9–27.9	$Pna2_1$	139.5	1.28	[1, 5, 22–24]
para	445	26.5–27.2	$R\overline{3}$	132.7	1.32	[1, 25, 26]

Table II: Summary of TM-DSC results at heating and cooling rates of 2 K min^{-1}: onsets of melting (T_m^{on}) and crystallization (T_c^{on}); enthalpy of melting (ΔH_m); and thermal-hysteresis parameters (ΔT_c and T_c/T_m). The last column corresponds to glass-transition temperatures measured with FSC, as discussed in more depth in the main text. Reported error bars correspond to one standard deviation.

Isomer	T_m^{on} (K)	T_c^{on} (K)	ΔH_m (kJ mol^{-1})	ΔT_c (K)	T_c/T_m	T_g (K)
ortho	378.0±0.1	312±4	19.3±0.3	66	0.83	248.5
meta	381.8±0.1	309±8	18.4±0.2	72	0.81	265
para	445.3±0.2	434.9±0.8	24.3±0.8	10	0.98	*

* No glass transition observed up to a cooling rate of 3000 K s^{-1}

Table III: Experimental(calculated) lattice parameters for the three dHBZ isomers in the the crystallographic phases reported in Table I above.

Isomer	**a** (Å)	**b** (Å)	**c** (Å)
ortho	9.751(9.971)	5.615(5.493)	10.351(10.712)
meta	10.469(10.467)	9.406(9.470)	5.665(5.632)
para	5.689(5.689)	38.180(38.180)	38.191(38.191)

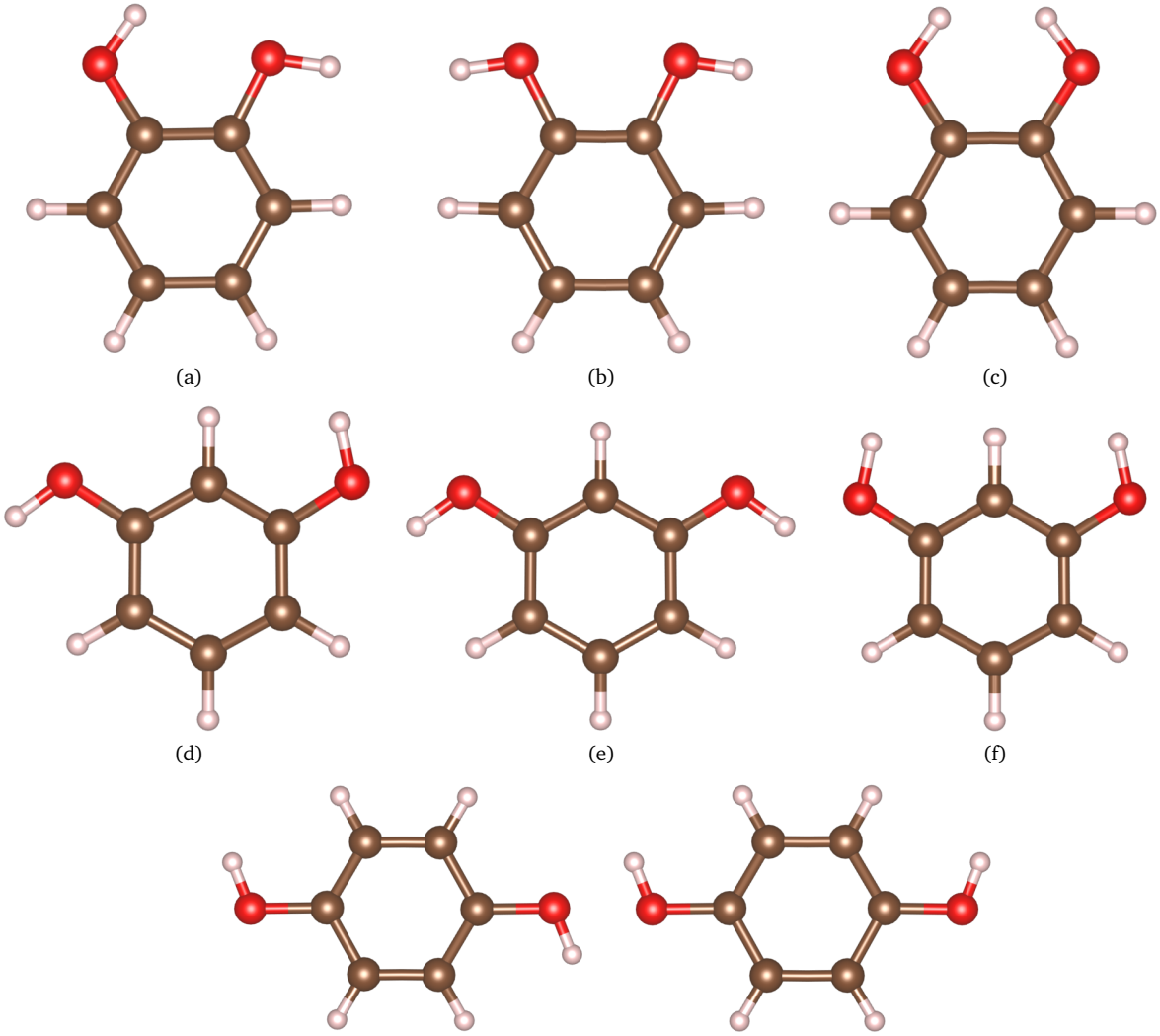

Figure S1: Planar conformers of *o*-dHBZ (top row, a-c), *m*-dHBZ (middle row, d-f) and *p*-dHBZ (bottom row, g-h). For further details, see the main text.

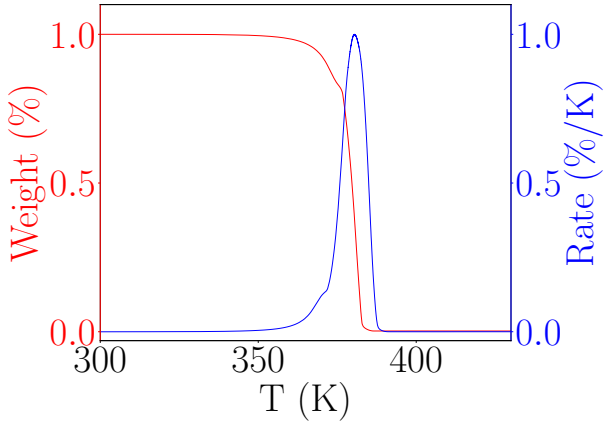

(a)

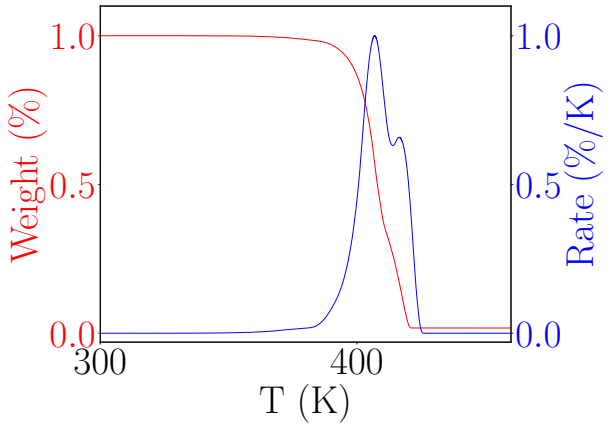

(b)

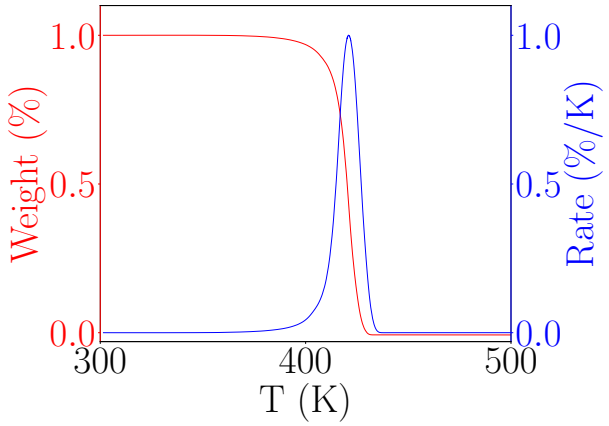

(c)

Figure S2: TGA data for *o*-dHBZ (a), *m*-dHBZ (b) and *p*-dHBZ (c). Left axis (red): % weight loss. Right axis (blue): first derivative of the % weight loss.

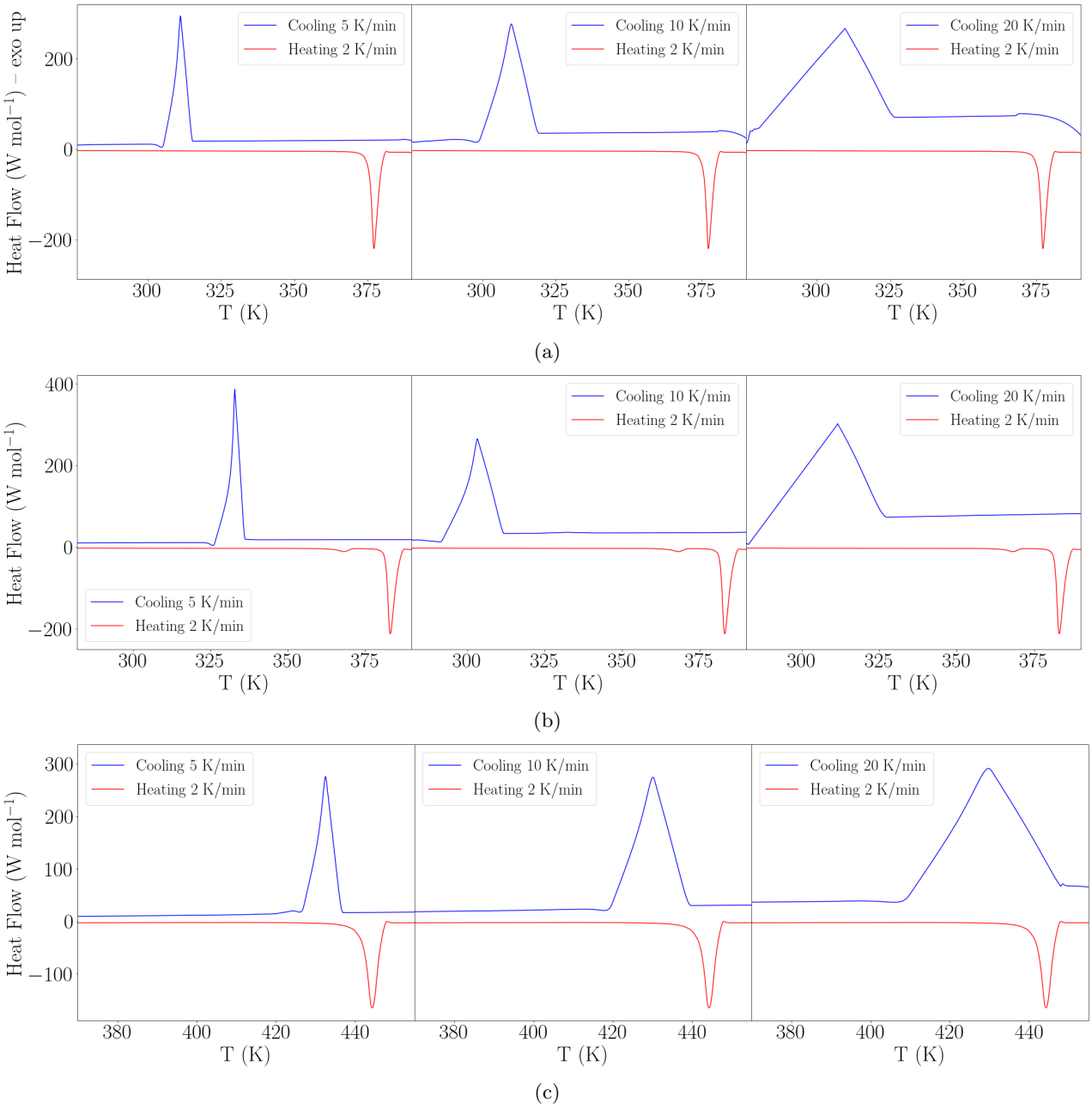

Figure S3: Comparison between TM-DSC scans of (a) *o*-dHBZ, (b) *m*-dHBZ and (c) *p*-dHBZ at a constant heating rate of 2 K min^{-1} (red) and varying cooling rates (blue).

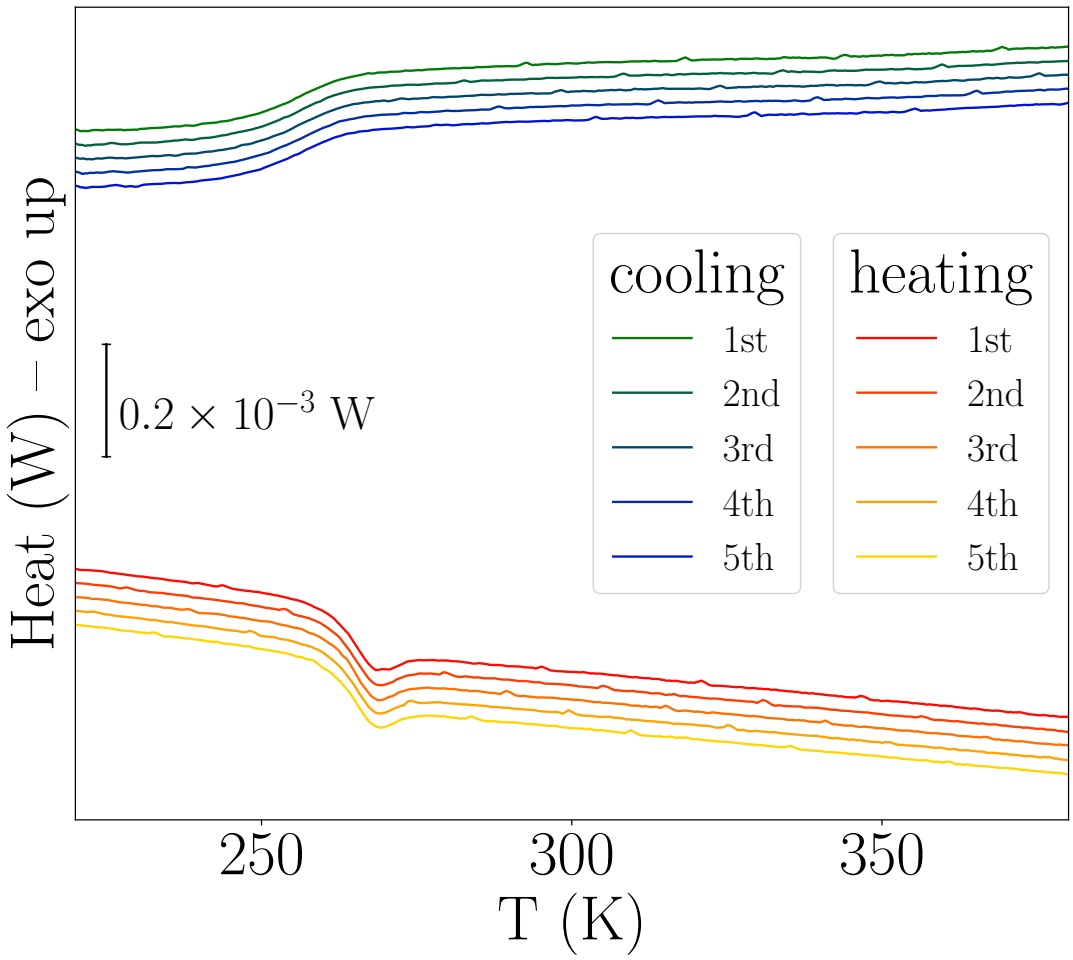

Figure S4: FSC curves of consecutive heating/cooling cycles for *m*-dHBZ at a fixed rate of 1000 K s^{-1}.

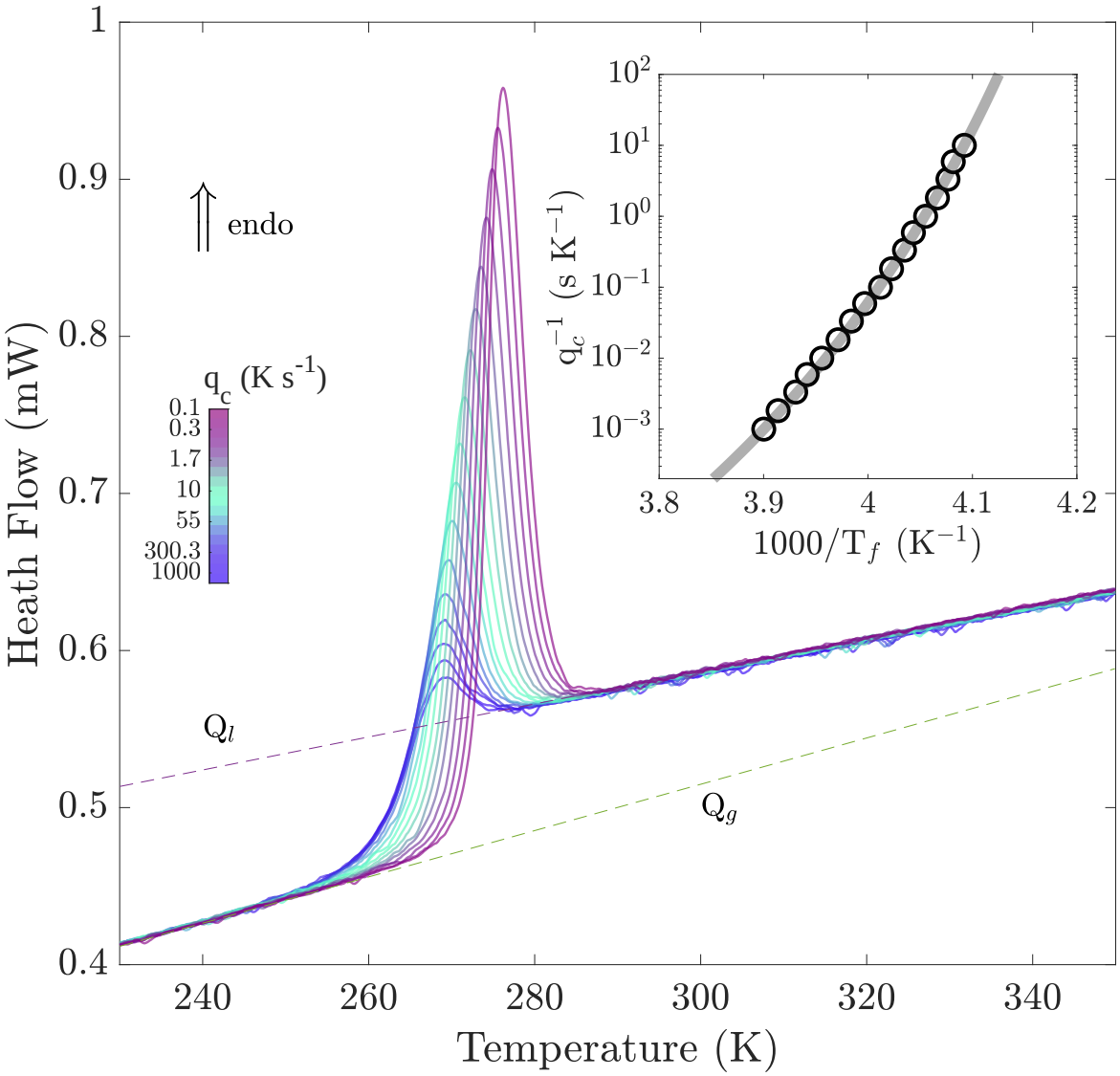

Figure S5: FSC scans of *m*-dHBZ around the glass transition using a heating rate of q_h=1000 K s^{-1}. Different cooling rates (q_c) are displayed with different colours from 0.1 to 1000 K s^{-1}. The baselines for glass (Q_g) and supercooled liquid (Q_l) are displayed as dashed lines. Inset: fictive temperatures as a function of the inverse of the cooling rate and VFT fit using Eq. (1) above (solid line).

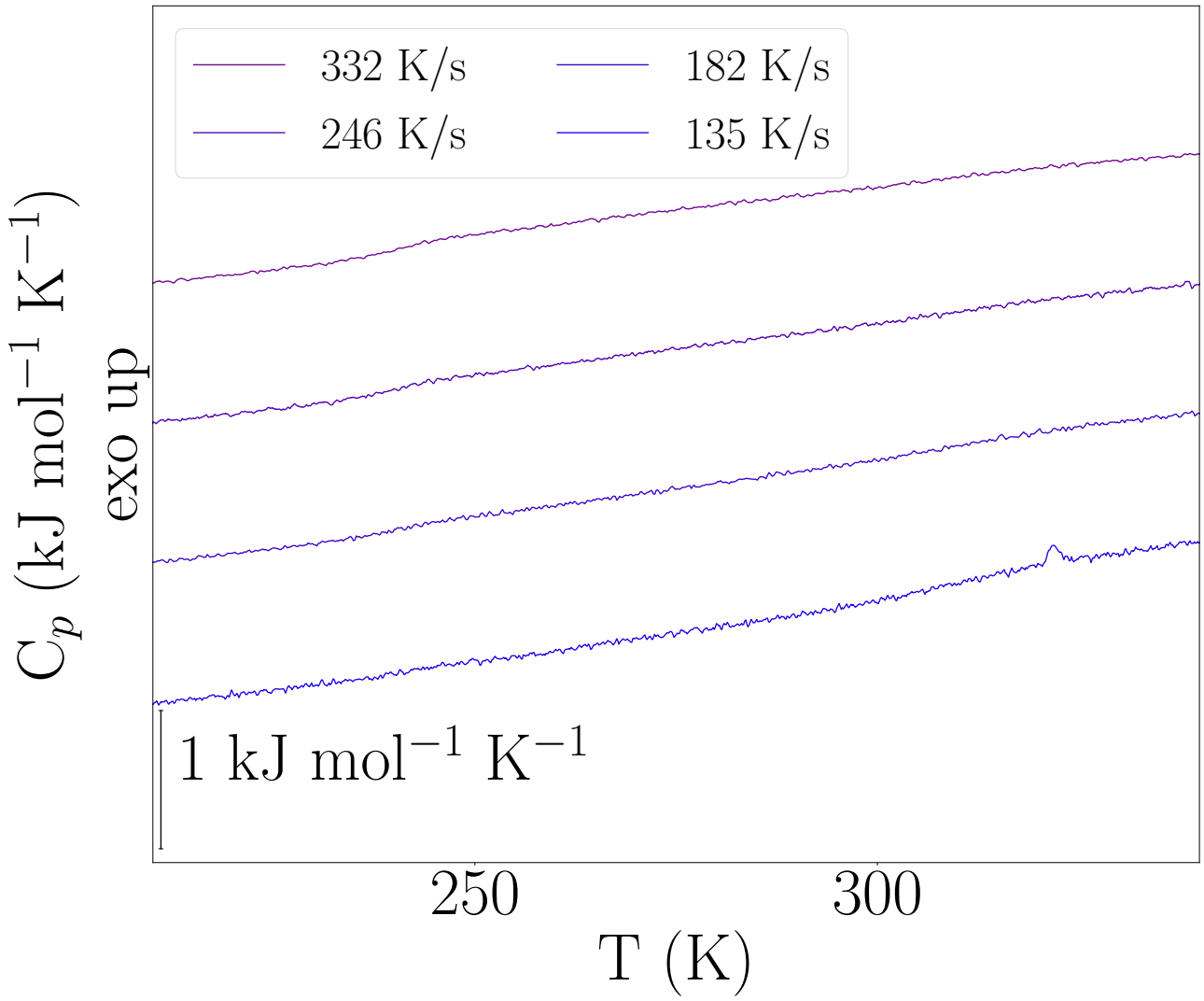

Figure S6: FSC curves of consecutive cooling cycles of *o*-dHBZ at different rates. At 135 K s^{-1}, the glass transition is no longer discernible and a weak crystallization peak is observed at 320 K.

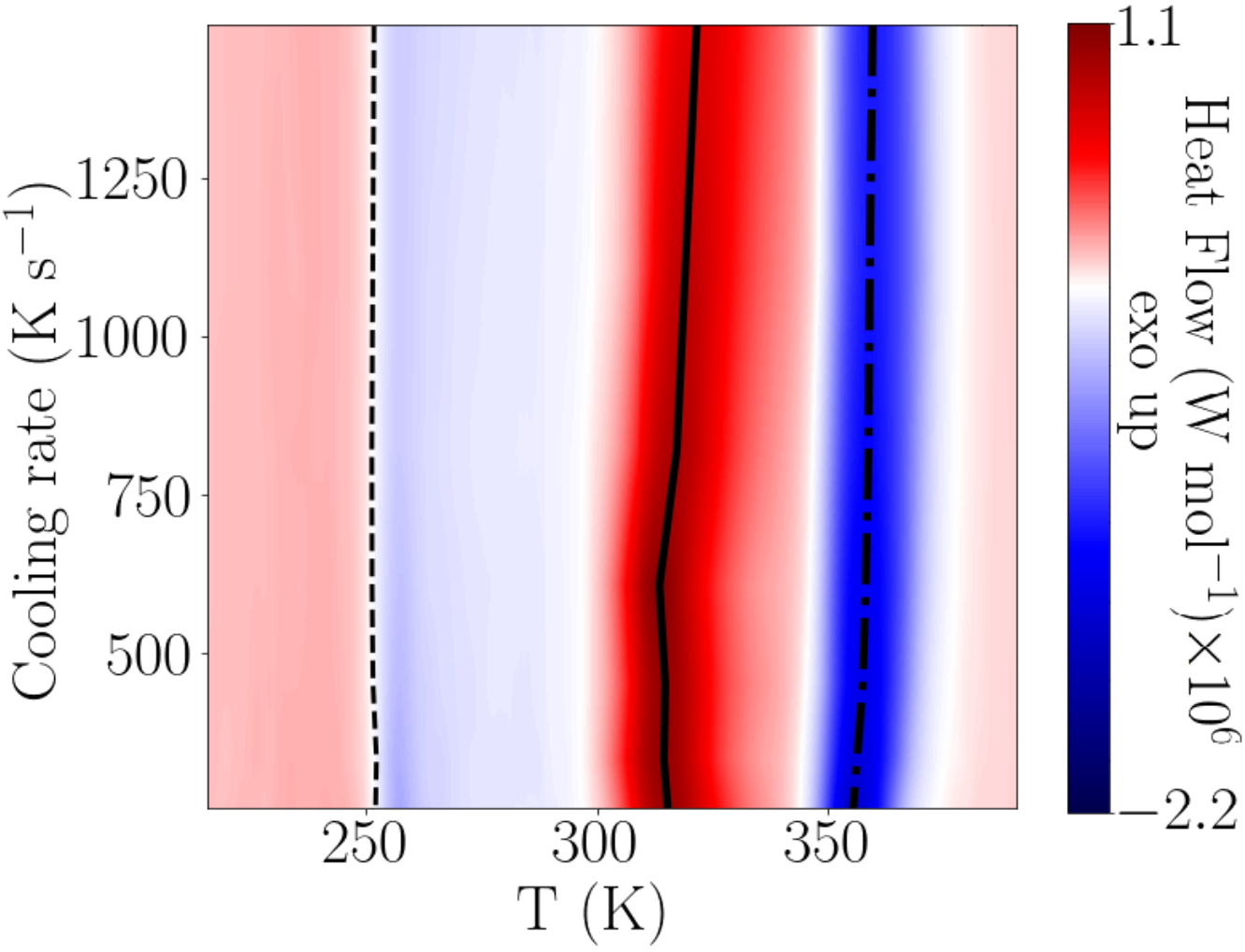

Figure S7: FSC colour map of *o*-dHBZ as a function of temperature (abscissa) and cooling rate (ordinate axis). The heating rate was fixed at the maximal value of 3000 K s^{-1}. The dashed, solid, and dashed-dotted lines indicate the evolution of T_g, T_{cc} and T_{m2} with cooling rate, respectively.

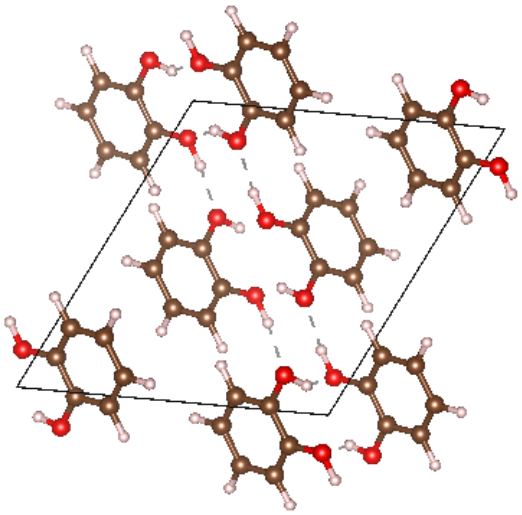

Figure S8: Crystal structure of *o*-dHBZ as reported in the literature – see Table I above. For further details, see Fig. 4 and accompanying discussion in the main text.

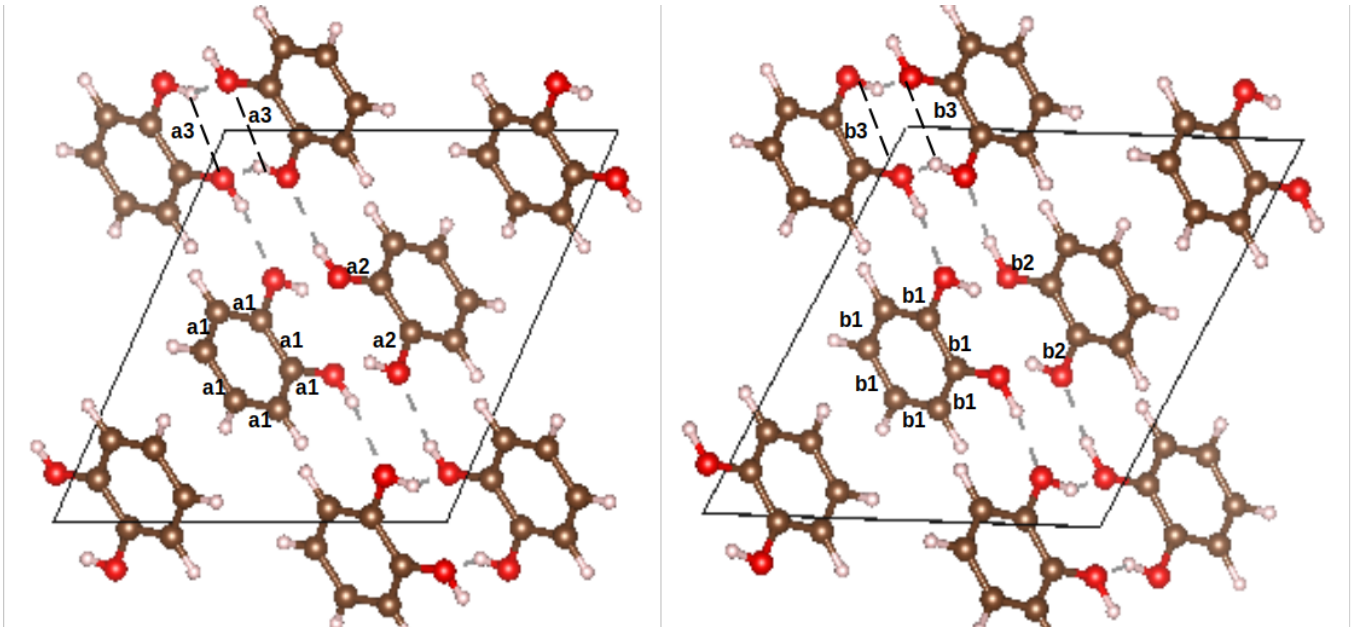

Figure S9: Experimental (left) and calculated (right) crystal structures of *o*-dHBZ. Relevant structural parameters are also included. For the experimental data, these correspond to: C-C bonds in the benzene ring, a1 = 1.391 Å; intramolecular C-O bonds, a2 = 1.374 Å; and intramolecular H-bonds, a3 = 2.273 Å. These values are to be compared with the computational predictions: b1 = 1.396 Å; b2 = 1.376 Å; and b3 = 2.308 Å.

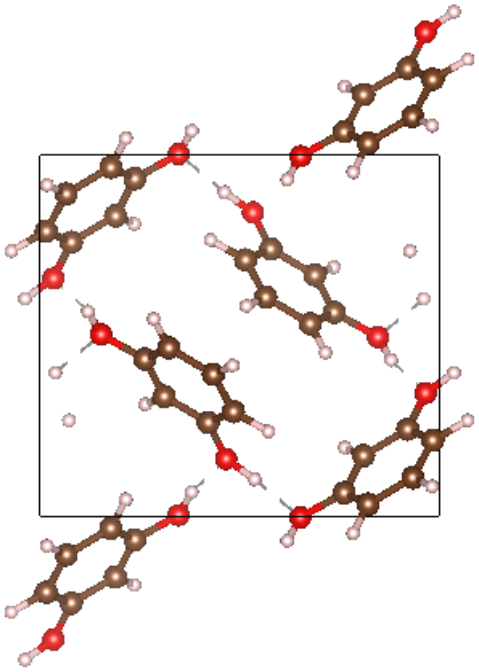

Figure S10: Crystal structure of *m*-dHBZ as reported in the literature – see Table I above.

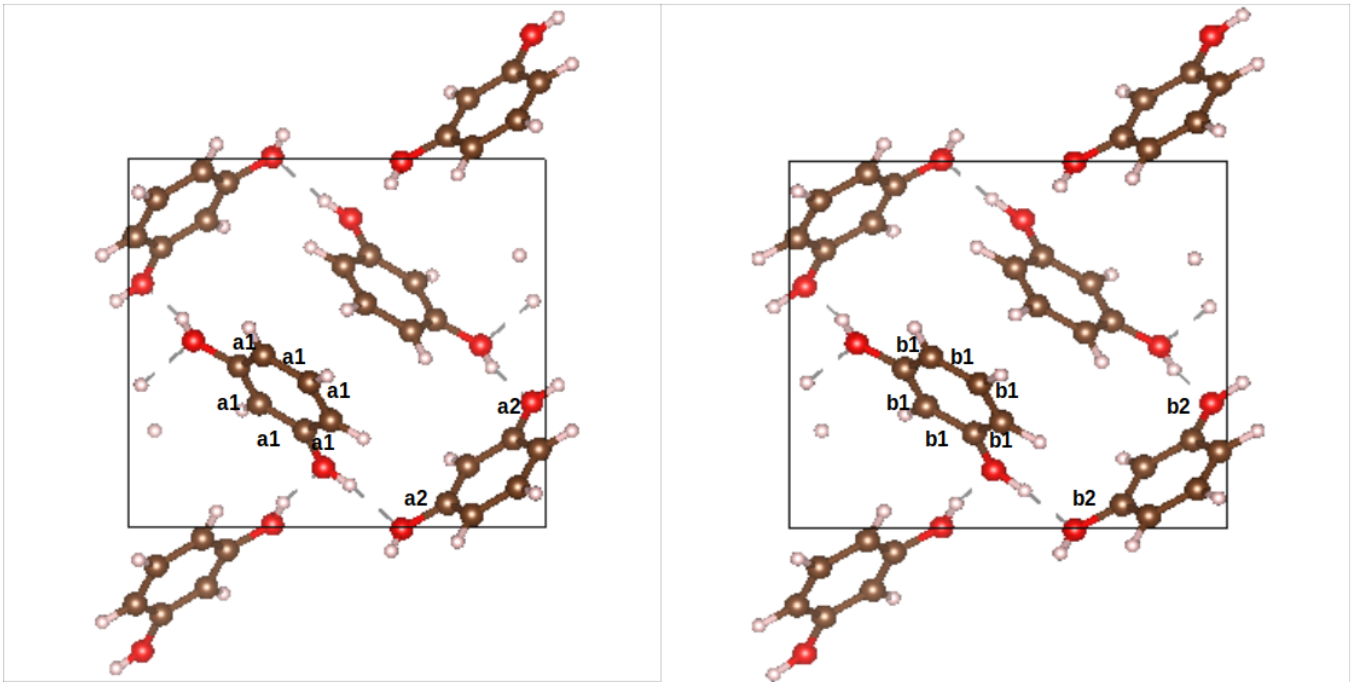

Figure S11: Experimental (left) and calculated (right) crystal structures of *m*-dHBZ. Relevant structural parameters are also included. For the experimental data, these correspond to: C-C bonds in the benzene ring, a1 = 1.390 Å; intramolecular C-O bonds, a2 = 1.377 Å. These values are to be compared with the computational predictions: b1 = 1.397 Å; b2 = 1.378 Å.

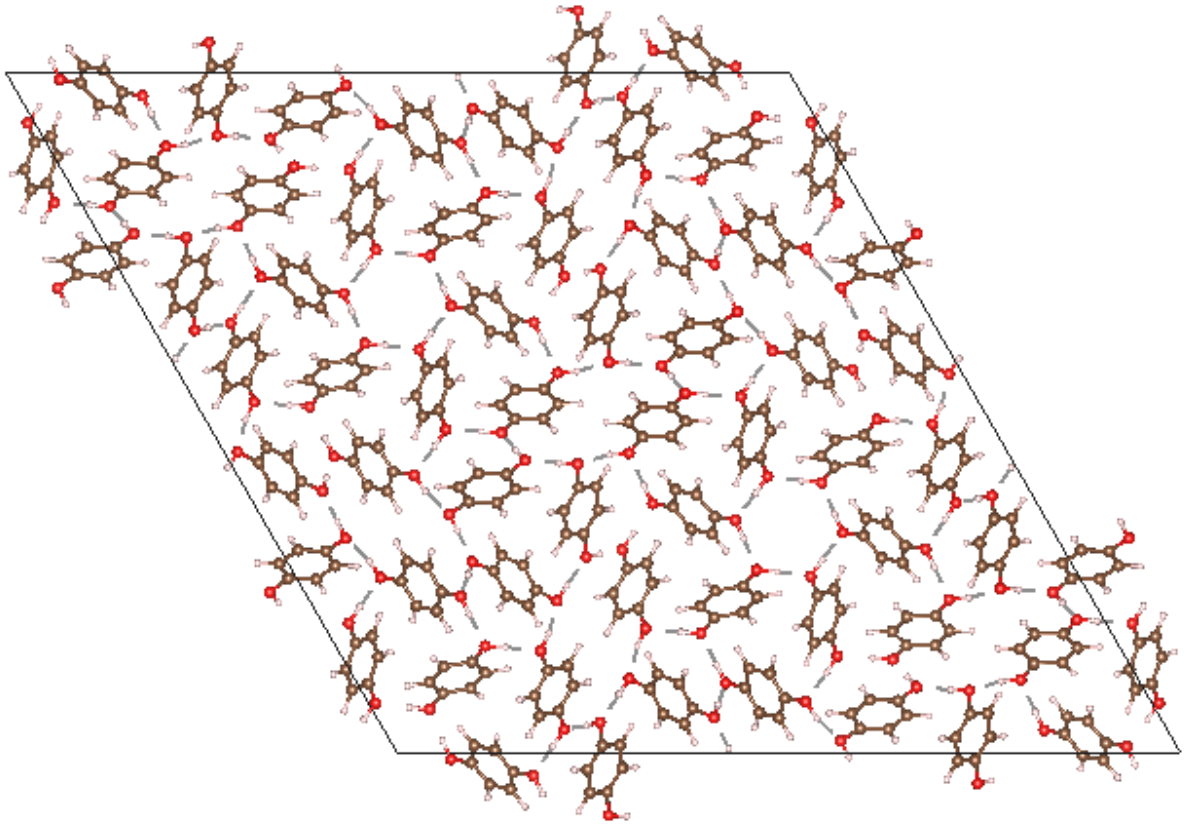

Figure S12: Crystal structure of *p*-dHBZ as reported in the literature – see Table I above.

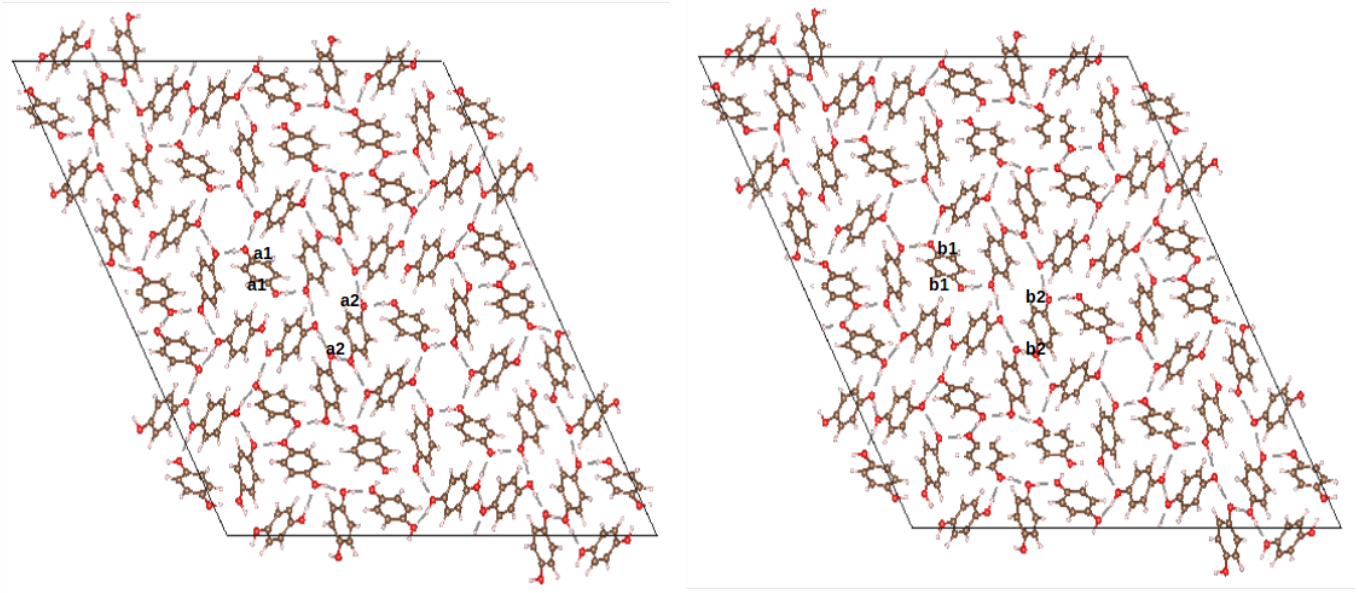

Figure S13: Experimental (left) and calculated (right) crystal structures of *m*-dHBZ. Relevant structural parameters are also included. For the experimental data, these correspond to: C-C bonds in the benzene ring, a1 = 1.397 Å; intramolecular C-O bonds, a2 = 1.380 Å. These values are to be compared with the computational predictions: b1 = 1.397 Å; b2 = 1.381 Å.

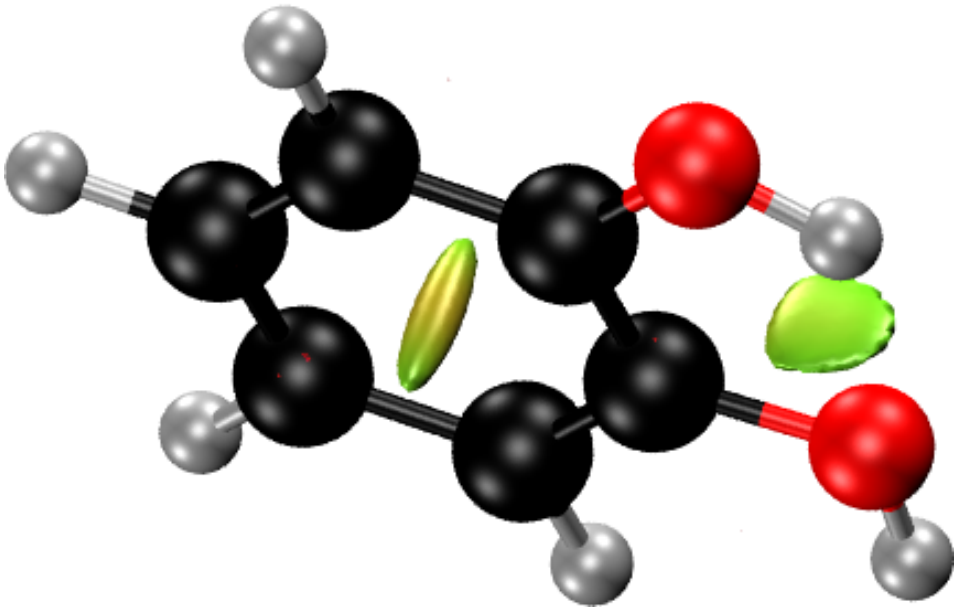

Figure S14: Calculated NCI domains for the *o*-dHBZ monomer, evincing the presence of intramolecular HB interactions in the isolated molecule.